RESEARCH ARTICLE

SOLID-STATE CHEMISTRY

Quantum and isotope effects in lithium metal

Graeme J. Ackland,[1] Mihindra Dunuwille,[2] Miguel Martinez-Canales,[1] Ingo Loa,[1] Rong Zhang,[2] Stanislav Sinogeikin,[3] Weizhao Cai,[2] Shanti Deemyad[2]*

The crystal structure of elements at zero pressure and temperature is the most fundamental information in condensed matter physics. For decades it has been believed that lithium, the simplest metallic element, has a complicated ground-state crystal structure. Using synchrotron x-ray diffraction in diamond anvil cells and multiscale simulations with density functional theory and molecular dynamics, we show that the previously accepted martensitic ground state is metastable. The actual ground state is face-centered cubic (fcc). We find that isotopes of lithium, under similar thermal paths, exhibit a considerable difference in martensitic transition temperature. Lithium exhibits nuclear quantum mechanical effects, serving as a metallic intermediate between helium, with its quantum effect–dominated structures, and the higher-mass elements. By disentangling the quantum kinetic complexities, we prove that fcc lithium is the ground state, and we synthesize it by decompression.

At ambient pressure, lithium is the lightest metal in the periodic table. We might expect that this would lead to simple chemistry of the electrons and complex quantum behavior of the nuclei. In fact, crystallography shows highly complicated structural behavior, and the isotope differences that could prove nuclear quantum effects have remained largely unstudied. Here we address both these issues, presenting a comprehensive picture of how the quantum interplay of the nuclei and electrons leads to surprising and hitherto unsuspected behavior in this simplest of metallic elements.

For light elements, the nuclear zero-point vibrations—a wholly quantum effect arising from the fact that the nuclei are never truly at rest—can be orders of magnitude larger than the very small energy differences between competing crystal structures (*1*). Quantum ground states are responsible for superconductivity and superfluid behavior, which allow flow of charge or matter without resistance. Quantum effects are especially pronounced in metallic systems of low mass at high densities, leading to extraordinary properties as well as exotic states of matter (*2*–*5*). The effects manifest as differences between isotopes. For example, ^{4}He is almost twice as dense as ^{3}He at the same pressure and temperature (*6*) and has a hexagonal rather than cubic crystal structure.

Away from ambient conditions of pressure and temperature, lithium exhibits unusual and complicated behavior, including numerous temperature- and pressure-induced phase transitions to low-symmetry structures (*7*), metal to semiconductor to metal transitions (*8*, *9*), both a maximum and a minimum temperature in its melting line (*10*, *11*), and superconductivity with an anomalous isotope effect (*12*–*15*). At room temperature and pressures below 7 GPa, ^{7}Li crystallizes in the body-centered cubic (bcc) structure. When cooled below $T \approx 77$ K (at $P = 0$ GPa), bcc ^{7}Li undergoes a martensitic transition to a close-packed structure (*16*), identified as the 9R structure (*17*, *18*), which has a nine-layer stacking sequence and has previously been assumed to be the ground-state structure. It is odd that a simple metal would adopt a complicated atomic arrangement at zero pressure, and despite much theoretical effort to understand the multifaceted physics underlying the small differences between the energies of various close-packed structures, there is no clear explanation in the literature [e.g., (*19*–*21*)].

The free energy landscape of materials often contains multiple local minima, and the critical role of quantum effects in controlling the kinetics of changing between them has only recently been recognized (*22*). Consequently, a proper determination of thermodynamic states requires care in identifying the *P*-*T* paths along which a phase diagram is constructed. Earlier high-pressure, low-temperature structural phase diagrams of lithium were constructed on the basis of few experimental studies that used only ^{7}Li (*7*, *23*, *24*). Lithium is an extremely challenging material for high-pressure studies: It reacts chemically with many materials (e.g., it causes gasket metals and diamonds to become brittle), and diffraction experiments are challenging because of low x-ray and neutron scattering cross sections.

Structural transitions: Experimental evidence

With only three electrons, lithium is a very weak scatterer of x-rays, and the low-temperature structures of lithium have mainly been studied by neutron scattering. However, because of the high neutron absorption cross section of ^{6}Li (940 barn), these studies have only been performed on ^{7}Li (0.0454 barn) [e.g., (*17*, *23*, *25*)]. Hence, the *P*-*T* structural phase diagram of ^{6}Li has not previously been reported. Moreover, the structural boundaries of ^{7}Li below 80 K were uncertain, especially with respect to transformations between the martensitic and face-centered cubic (fcc) phases. Because of advances in synchrotron beam quality, diamond anvil pressure cells can be used to investigate the low-temperature and high-pressure regions of the lithium phase diagram (*26*).

We observed a large difference between the martensitic transition in the ^{6}Li and ^{7}Li samples under similar conditions (Fig. 1), contrary to early ambient-pressure studies (*26*–*28*). We found that the ^{6}Li samples did not show any evidence of a martensitic transition or any other structural phase transitions during isobaric cooling between 0.2 and 2.0 GPa (Figs. 1A and 2A). They remained in the pure bcc structure down to the lowest temperature we measured (~16 K), regardless of whether we used helium or mineral oil as the pressure medium. Cooling ^{7}Li at pressures below 3.3 ± 0.3 GPa always resulted in the appearance of martensite peaks mixed with bcc peaks below 75 K. For ^{6}Li we first observed evidence of a transformation from the bcc phase to the martensitic phase at ~20 K and ~2 GPa during both isobaric cooling and isothermal compression. With further pressurization of the ^{6}Li sample to ≥4.5 GPa at $T = 20$ K, we observed the appearance of additional fcc peaks (fig. S2).

Under hydrostatic conditions during isobaric cooling to low temperature, bcc ^{7}Li transformed to fcc at pressures higher than 3.3 ± 0.3 GPa. This finding removes an ambiguity in the previous boundaries of the fcc and martensitic states (*23*). For ^{6}Li, the point at which bcc transforms to fcc was above 4.0 GPa (Fig. 1A). These boundaries based on isobaric cooling do not always match up with the results from isothermal compression. The fcc structure always remained stable during isobaric cooling (Fig. 1, A and B); unlike the bcc structure, it did not undergo a martensitic transformation. We found that the critical pressure for bcc → fcc at room temperature was independent of the isotopic mass.

We observed that the pressure onset of phase transitions that include low-temperature paths depended strongly on the specific temperature-pressure path taken (*26*). For example, reaching ~3.5 GPa and ~20 K during isothermal compression of the ^{7}Li sample led to mixed bcc and martensitic structures (Fig. 1B, data point 3), whereas during isobaric cooling to the same *P*-*T* point, no evidence of the martensite was

[1]Scottish Universities Physics Alliance (SUPA), School of Physics and Astronomy and Centre for Science at Extreme Conditions, University of Edinburgh, Edinburgh EH9 3FD, UK. [2]Department of Physics and Astronomy, University of Utah, Salt Lake City, UT 84112, USA. [3]High Pressure Collaborative Access Team (HPCAT), Geophysical Laboratory, Carnegie Institution of Washington, Argonne, IL 60439, USA.
*Corresponding author. Email: deemyad@physics.utah.edu

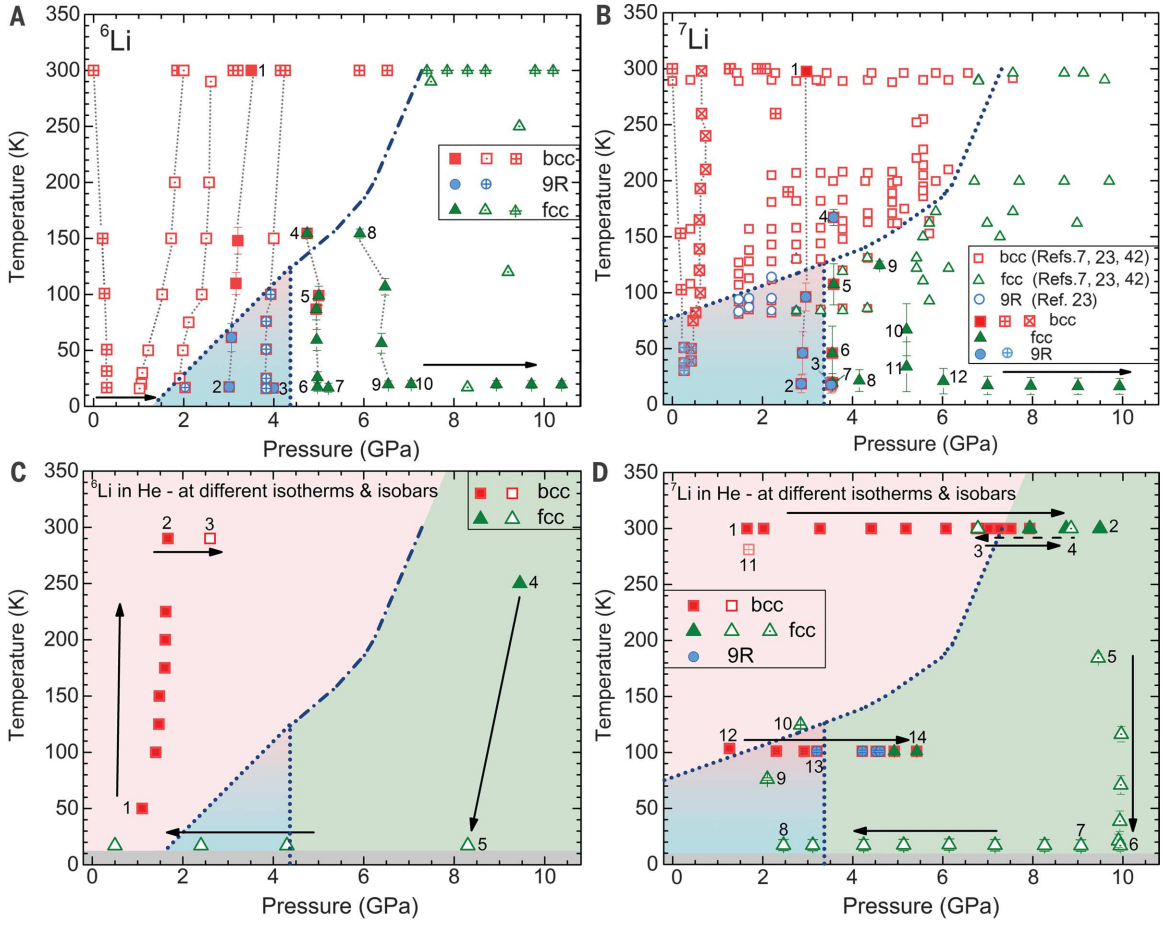

Fig. 1. Observed stable and metastable crystal structures of ^{6}Li and ^{7}Li measured along the identified *P-T* paths. (**A**) Isobaric results for ^{6}Li. Isobaric cooling paths are connected by gray lines as guides to eye. Data points collected during isothermal compression or isobaric warming are labeled in numerical order. We used mineral oil (crossed symbols) or He (dotted and solid symbols) as pressure-transmitting media. Blue dotted lines show the onset of bcc → close-packed transitions upon cooling. The dot-dashed line shows the tentative bcc-fcc boundary based on the limited data available for this region. (**B**) Isobaric results for ^{7}Li. Open symbols are data from previous studies that used either mineral oil or no pressure medium during isothermal compression and isobaric cooling (*7*, *23*, *42*). Points 3 and 7 are very close in *P* and *T* but were approached via different thermal paths; the resulting structures are 9R + bcc and fcc + bcc, respectively. (**C**) Experimental paths for ^{6}Li in *P-T* space to examine the possibility of a reverse fcc → 9R transformation during decompression. Dotted and dot-dashed lines are the transition lines from (A). During decompression, we observed the pure fcc structure deep in what was previously identified as the 9R stability region. (**D**) Experimental paths for ^{7}Li in *P-T* space with the same observation of the fcc structure in the 9R stability region. Dotted lines are the transition lines from (B). Points 12 to 14 show the martensitic transition of ^{7}Li during isothermal compression, followed by a transition to fcc. Error bars in all panels denote the estimated experimental uncertainty in the temperature of the sample and are comparable to the symbol size where not shown.

observed, and instead the sample crystallized in fcc + bcc (Fig. 1B, data point 7). We found (Fig. 1 and figs. S6 and S7) that the martensitic phase was only ever obtained from bcc → martensite transformations. Although transitions from martensite to fcc were seen, the reverse process never occurred.

Of particular interest is the *P-T* path shown in Fig. 1D, where we pressurized the bcc ^{7}Li sample at ambient temperature to >8 GPa to produce fcc and then cycled back across the phase boundary to demonstrate low hysteresis. We then cooled the sample to 20 K at ~10 GPa and depressurized it to 2 GPa, accessing the region previously ascribed to the 9R phase. We then warmed the sample to 120 K, which is above the reported 9R phase boundary (*23*). The sample remained fcc throughout this path. Further warming to room temperature induced a transition back to bcc. Finally, we cooled the sample back to 100 K and repressurized it until the martensitic phase appeared above 3 GPa. A similar result was found for ^{6}Li, where we synthesized the fcc ground state by pressurizing to 9 GPa, cooling to 20 K, then depressurizing to ambient pressure (Fig. 1C).

Explaining the 9R-martensite transition

The 9R structure was believed to be the ground state of lithium on the basis of the reproducibility of diffraction patterns from ambient-pressure isobaric-cooling studies (*17*, *18*, *25*, *26*, *29*); fcc was ignored by theorists, even in high-pressure work (*30*–*35*). The martensite has a well-defined crystal structure and it cannot be dismissed as a highly defective version of something simpler (*24*). However, the observed bcc → 9R transition does not prove the existence of a phase boundary because it is not reversible. Upon heating, the martensite transforms to fcc before returning to bcc (Fig. 3A) (*29*).

We performed well-converged free energy calculations using all-electron density functional theory (DFT) and the quasiharmonic approximation for phonons (QHA) (*26*). We found stable phonons as well as free electron–like band structures and Fermi surfaces for all phases up to 5 GPa (*26*). Additional calculations using the SCAILD method (*36*) showed that anharmonic effects are negligible at these temperatures (fig. S11). The DFT calculations reveal a fcc ground state. The bcc structure is stable at high temperature and low pressure because it has higher entropy and volume. The fcc → bcc transition temperature we calculated increases with pressure (Fig. 3), and the value of 166 ± 10 K at zero pressure is in good agreement with the reported values for the retransformation upon heating (*16*, *18*, *21*, *29*, *37*).

The 9R phase is always unstable with respect to fcc and other close-packed stackings such as hexagonal close-packed (hcp). Our calculations show that 9R becomes stable relative to bcc at 80 K and 0 GPa, with the phase boundary rising with pressure. To reconcile these DFT results with the experimental observation of the martensite, we directly simulated the martensitic transformation. This required modeling very large numbers of atoms with molecular dynamics (MD), which is currently unfeasible using DFT. We therefore derived a bespoke many-body interatomic potential (*26*) fitted directly to the relevant DFT properties. The new potential reproduces the DFT phase behavior (with fcc being the

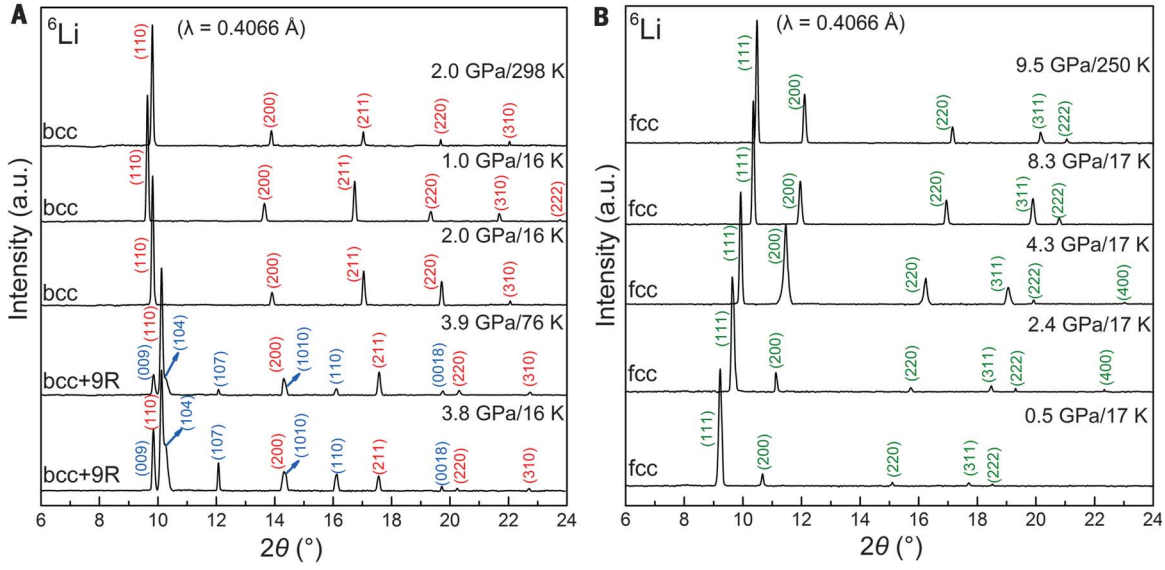

Fig. 2. Synchrotron x-ray diffraction patterns of ^{6}Li at different pressures and temperatures. Angle-dispersive diffraction measurements were performed using a wavelength of 0.4066 Å. (**A**) Selected diffraction patterns of ^{6}Li from three different cooling paths (points 1 → 4, 8 → 10, and 11 → 13 in fig. S6). The reflections from bcc (red) and martensitic (blue) phases are labeled by their *hkl* indices, using the 9R structure for the martensite. Not all 9R peaks are visible because the sample recrystallized to a highly textured quasi–single crystal. (**B**) Diffraction patterns of ^{6}Li during cooling to the base temperature, 17 K, and isothermal decompression to 0.5 GPa (points 18 → 22 in fig. S6). Only the pure fcc phase (green) was observed (Fig. 2). For clarity, the Compton scattering of the diamonds and reflections from the cryostat window have been removed in both (A) and (B). The data at 4.3 GPa show line broadening consistent with nonhydrostatic strain of up to 1%. This is likely due to a partial escape of the helium pressure-transmitting medium as the pressure on the cell was released.

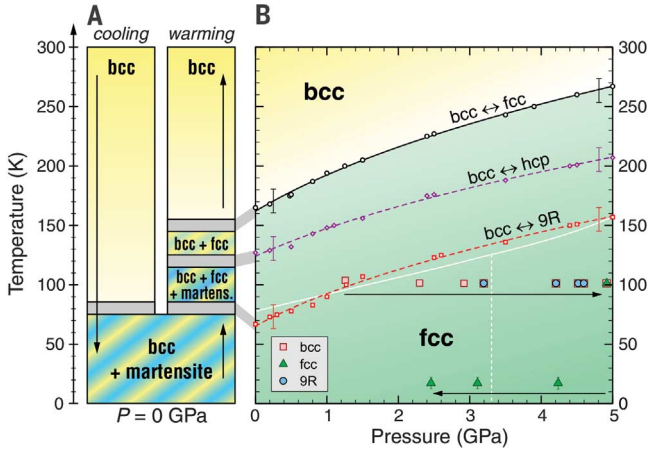

Fig. 3. Phase transitions in lithium as a function of pressure and temperature. (**A**) Experimental observations of bcc, fcc, and martensitic (9R and disordered) polytypes of ^{7}Li upon cooling and warming at zero pressure (*16*, *18*, *21*, *29*, *37*). (**B**) Calculated thermodynamic phase boundary between bcc and fcc, and metastable bcc-hcp and bcc-9R boundaries. Small symbols indicate the DFT results for ^{7}Li; the corresponding lines are interpolations. The corresponding ^{6}Li lines are a few kelvin lower (fig. S16). White lines indicate the experimental transition lines of ^{7}Li during isobaric cooling from this work and (*24*). Large symbols show the observed phases upon isothermal pressure changes (Fig. 1D). We can relate the calculated phase boundaries to the temperature-driven transitions at zero pressure [gray bars connecting (A) and (B)]. The equilibrium phase diagram contains only bcc and fcc; the solid black line represents the only phase boundary in this region of *P-T* space.

thermodynamically stable phase at low temperature and pressure) as well as the lattice parameters and elastic properties of relevant phases. As with DFT, the potential model shows that the bcc phase is entropically stabilized over fcc above ~150 K.

We used the large-scale MD simulations to simulate the cooling transition (*26*). We used 128,000 atoms, starting with either a bcc single crystal or bcc nanocrystals, and cooled them into the region of fcc stability. We observed transformations to a twinned, close-packed structure that is neither fcc nor pure 9R (Fig. 4A). The apparent contradiction between the known fcc ground state of the potential and the observed martensite means that the bcc → fcc transition is kinetically hindered, and that a transition can only occur once all close-packed stackings are favored relative to bcc. Experimentally, the bcc → 9R transition is always incomplete, so the remnant bcc material in the sample provides nucleation sites for retransformation. Analyzing the stacking sequences of the largest twins leads to the surprising result that the stacking is nonrandom and has significantly more hcp-like *h* layers than fcc-like *k* layers. The 9R-like, three-layer *hhk* motif is prominent (Fig. 4A).

Using the Debye method, we simulated the powder neutron diffraction patterns for the three main twins generated in the MD simulation (Fig. 5). We compared these simulations with the best ambient-pressure neutron diffraction experimental data (*38*). Our simulated diffraction patterns for the martensite twins show all of the features observed in the experiment without any fitting. The simulated martensitic patterns yield a better approximation of the experimental data than does the 9R structure itself. This includes the shift and broadening of the (1 0 4), (0 1 5), (1 0 13), and (0 1 14) reflections relative to the ideal 9R prediction, and the suppression of peak intensities in the 34° to 48° region. Because the stacking sequences extracted from the MD simulation comprise only 21 to 47 layers, the simulated patterns from single twins show signs of finite-size effects; most notably, the (1 0 13) and (0 1 14) reflections in the largest twin pattern are less broadened and shifted more with respect to the ideal 9R pattern than observed in the experiment. However, the three-twin average already shows a much better agreement with the experiment. Fits to the experiment of similar quality to ours can only be achieved by postulating an appropriate concentration of stacking faults within the 9R structure (*38*).

The excellent agreement between the simulated and experimental patterns shows that the martensite obtained in the MD simulation correctly describes the experimentally observed structure. The discrepancies between the ideal 9R diffraction pattern and the experimental data have been noted before and can be explained by postulating an appropriate concentration of stacking faults within the 9R structure (*18*, *29*, *37*, *38*).

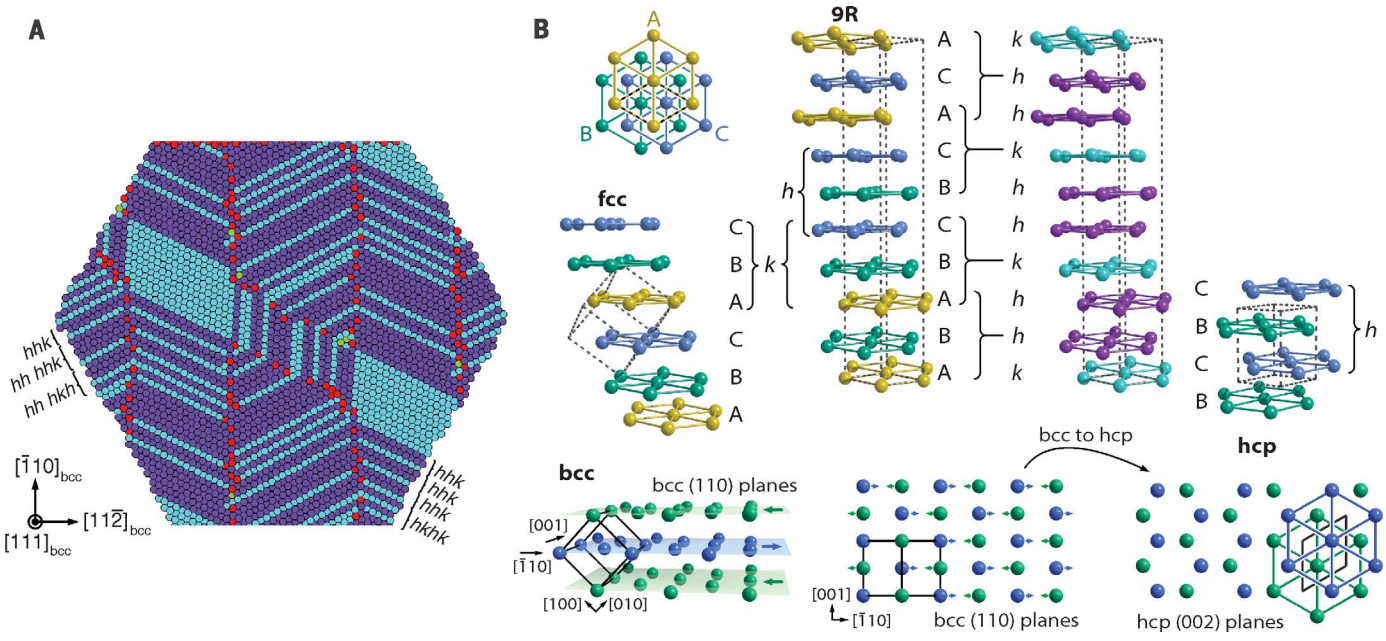

Fig. 4. Structures of lithium. (**A**) Complex, non-9R stacking sequence in the martensite from the MD simulations, viewed along the $[111]_{bcc}$ body diagonal from the initial bcc crystal. The close-packed layers are shown edge-on, exposing the stacking sequence. Atoms with a local hcp (*h*) or fcc (*k*) environment are shown in dark purple and cyan, respectively (*43*). Other colors mark atoms without close-packed coordination at cell and grain boundaries. There are three separate twins, as well as a region of pure fcc (which is a known finite-size effect) (*44*). Such fcc regions form only in MD cells with orientations incompatible with a two-twin microstructure. MD simulations in supercells rotated 45° about $[100]_{bcc}$ produced microstructures with only two twins. Simulations starting with bcc nanocrystals produced an ultrafine twinned microstructure that coarsened slowly. Simulations with high cooling rates remained in bcc. (**B**) Relationship among fcc, hcp, 9R, and bcc. Top: The close-packed structures can be identified by their stacking sequences of hexagonal layers along the *z* axis. In the ABC notation, the letters refer to different atomic positions in the *xy* plane. The *hk* notation removes the arbitrary choice of origin and labels a layer as hexagonal (*h*) if the layers directly above and below the central layer are of the same type, and as cubic (*k*) otherwise. The sequence ABACACBCB for the 9R structure translates to *hhk hhk hhk*. Unit cells are indicated with dark dashed lines. Bottom: Illustration of the martensitic mechanism in which the bcc $(110)_{bcc}$ layers of atoms transform into close-packed $(001)_{hcp}$ layers and shuffle into the appropriate stacking sequence, shown here for the bcc → hcp transformation. The bcc → fcc transition requires a substantial shear strain parallel to (110), three times that required for the transition to 9R.

However, the key point is that our patterns are generated ab initio, without adjustable parameters or any reference to 9R. Our structure arises from the transformation kinetics, not the thermodynamic stability. Absence of the reverse transformation, from fcc to bcc or a martensitic structure, during the isothermal decompression at low temperature is precisely what we theoretically predict to occur (Fig. 1, C and D). We conclude that the diffusive bcc → fcc transition has no low-energy path, so instead bcc undergoes a martensitic transition with large hysteresis on both isobaric and isothermal paths. In other words, not only is the previously reported martensite not thermodynamically stable, it does not have the 9R crystal structure either.

Isotope and quantum effects

In classical thermodynamics, free energy differences between phases are independent of the nuclear mass, but at low temperatures, quantum effects can lead to differences in behavior for different isotopes because both vibrational and zero-point effects are dependent on mass. In lithium, the zero-point energy is large at ~40 meV per atom, equivalent to 500 K. The zero-point energy is larger in ^{6}Li than in ^{7}Li by a factor of $\sqrt{7/6}$. Early ambient-pressure measurements showed that at low temperature, ^{6}Li has a slightly larger bcc lattice constant (*28*). Also, isotope effects in the shear modulus in lithium under pressure are evidence of the quantum contribution (*3*, *39*). Although the zero-point energy of lithium has a large contribution to the vibrational energies and may influence high-pressure structures (*3*, *35*), the calculations do not suggest a major shift of the martensitic metastability limit between the two isotopes.

Entropy differences between phases ultimately drive thermal phase transitions, but the kinetics of the transition can prevent some transformations. The MD simulations demonstrated that the martensitic transformation path is complicated by the need to generate many different stackings. We therefore postulate that the transformation begins only when all close-packed stackings are stable against bcc. Because 9R is the least favorable stacking we have found, we associate the observed martensitic transition with the *P*-*T* conditions where 9R becomes more stable than bcc (Fig. 3B).

We approached this issue with DFT calculations and the QHA for the vibrational properties. The fcc equation of state (Fig. 6) allows a direct comparison between measurements and calculations uncompromised by hysteresis; we find that ^{6}Li is at a larger pressure for a given lattice parameter at low temperature (fig. S13), consistent with ambient-pressure experiments (*28*), and that it has a lower compressibility than ^{7}Li. Zero-point effects contribute to the pressure, so that a higher pressure is required to compress ^{6}Li to the same volume as ^{7}Li. Our calculations show that this implies a difference of ~25 MPa in the equation of state. The 9R structure is always thermodynamically unstable with respect to fcc, whereas bcc is stabilized at higher temperatures by vibrational effects. However, the isotope effect only shifts the phase boundary by a few degrees, so the thermodynamics indicates that fcc is the stable phase in ^{6}Li at low temperature, as seen in the depressurization experiments but not upon cooling. The observed survival of bcc to zero temperature might be due to a quantum kinetic effect. This is not implausible: Whereas the isotope effects in thermodynamics scale with the square root of the mass difference, in the kinetics, the rate depends exponentially on the mass via the higher zero-point energy contribution to the transition-barrier free energy of ^{6}Li. In principle, this could be tackled using large-scale ab initio path integral molecular dynamics, which includes both tunneling and zero-point effects, but such a calculation is currently intractable.

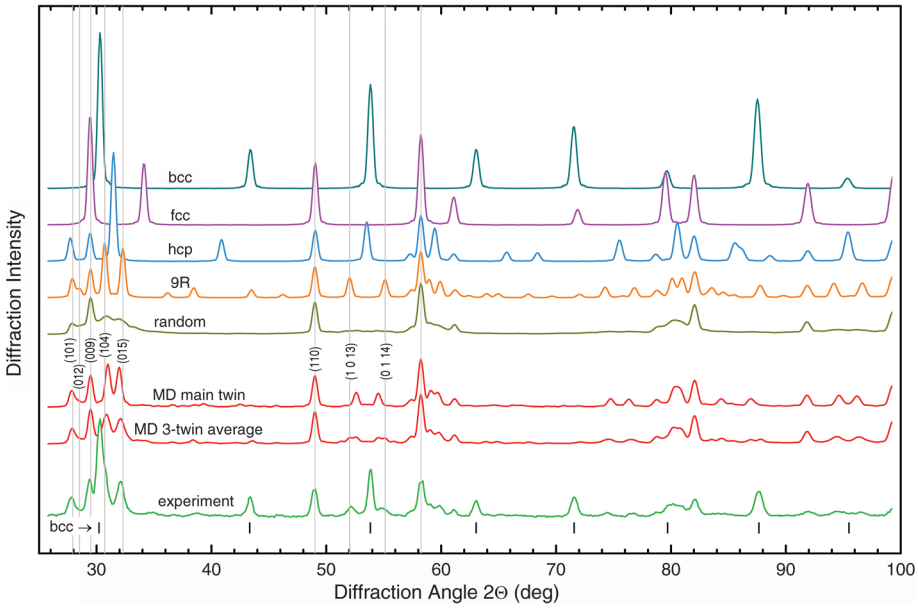

Fig. 5. Simulated diffraction patterns of lithium. Comparison of neutron diffraction data (wavelength λ = 1.288 Å) from ^{7}Li at T < 20 K and zero pressure (*38*) with simulated diffraction patterns from (top to bottom) various candidate phases of lithium, a random sequence of close-packed layers, the stacking sequence of the main twin obtained in the MD simulation, and an unweighted average of all three stacking sequences observed in the simulated martensite shown in Fig. 4A. The neutron diffraction pattern is a combination of bcc and martensite; the positions of the bcc peaks are replicated by the tick marks at the bottom. The Miller indices refer to the 9R structure.

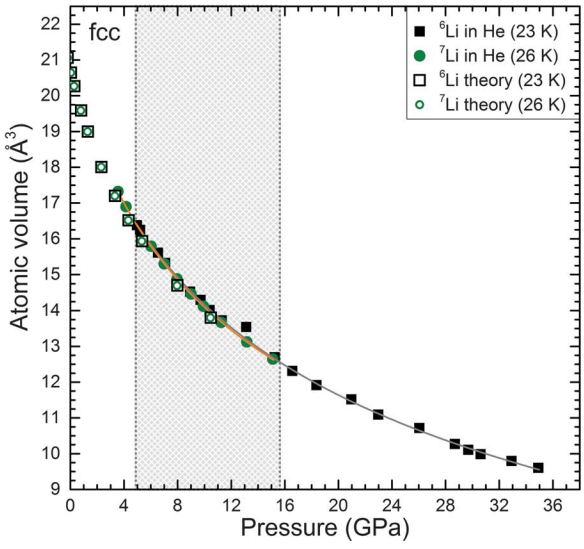

Fig. 6. Equations of state for fcc ^{6}Li and ^{7}Li. The atomic volume of the fcc phase of ^{6}Li and ^{7}Li at low temperature is plotted as a function of pressure, showing agreement of experiment and theory. The orange and gray lines indicate the third-order Birch-Murnaghan equation of state fits to the data from ^{7}Li and ^{6}Li, respectively, in the region where data were obtained for both isotopes (shaded region). Open symbols show the calculated equation of state for the lithium isotopes in the fcc phase. See (*26*) for details of all equations of state.

Martensitic transitions were reported to be sensitive to impurities and intrinsic defects such as vacancies in several systems (*40*, *41*). Although our samples show very similar impurity levels (*26*), contributions from slight differences between the impurity levels of the samples, below our resolution, cannot be entirely excluded. However, the similarity in the martensitic transition of ^{7}Li and natural lithium samples, regardless of their source and purity levels, as reported by many groups including ours, indicates that the observed phenomenon here is mass-related.

To understand the extent to which mass can affect the stability of lithium, we looked at the extreme, unphysical case of ^{3}Li and ^{14}Li, neither of which exists naturally. Whereas the bcc → fcc transition shows only a very small mass dependence, the bcc → 9R transition shows a very strong mass dependence, and the 9R phase would be entirely suppressed for ^{3}Li up to 1.2 GPa (fig. S16). These results qualitatively resemble our experimental observations for stable isotopes of lithium, albeit for unphysical masses. The stability line obeys the third law of thermodynamics, which requires that the phase boundary must become vertical if it approaches the T = 0 K axis. This makes it extremely sensitive to small changes in the energy difference between bcc and martensite: If the real martensite has a higher enthalpy than 9R, then the zero-point energy may be enough to destabilize it in ^{6}Li (*22*).

Metastability regions

Although 9R is not a stable phase of lithium and can only be obtained starting from bcc, the conditions where this occurs are reproducible and isotope-dependent. Under hydrostatic conditions, the bcc → 9R transition occurred at lower temperature and higher pressure in the ^{6}Li samples. By contrast, the transition line 9R → fcc appears to be at higher pressure in ^{6}Li: As discussed above, the 9R → fcc crossover pressure for isobaric cooling is 3.3 ± 0.3 GPa for the ^{7}Li material and at least 4.0 GPa for the ^{6}Li material. This suggests that the role of quantum effects is to inhibit the transition rather than to destabilize the 9R phase.

Combining these observations with the DFT results suggests that there are two important lines on the phase diagram (Fig. 3B): the true thermodynamic phase boundary between bcc and fcc, and a line designating conditions at which bcc is unstable with respect to any close-packed stacking sequence. The second line denotes the onset of the martensitic transformation mechanism, and it is the one observed in experiments. The ground state of lithium can be synthesized if this martensite line is avoided via a high-pressure path.

The structure of lithium

The experimental and calculated properties of lithium can be seen in a consistent manner that rewrites the understanding of this simplest of metals. In both ^{6}Li and ^{7}Li, the ground-state structure is fcc rather than 9R. A combination of zero-point energy and vibrational entropy stabilizes the bcc structure where it exists. Only the transition from bcc creates a metastable martensite, as it does not result from the structure's thermodynamic stability. A natural question that arises is whether the 9R states observed in other elements (e.g., Na, Sm) and alloys are thermodynamically stable phases.

In contrast to ^{7}Li, we observed that in the ^{6}Li samples, the bcc structure remained stable, relative to the martensite, down to the lowest measured temperatures for pressures up to ~2 GPa. The difference between ^{6}Li and ^{7}Li cannot be explained by thermodynamic calculations, and it indicates that quantum effects may play a crucial role in the transition kinetics.

We have synthesized the ground state of lithium in both isotopes using a high-pressure pathway to circumvent the martensitic transition.

REFERENCES AND NOTES

1. N. W. Ashcroft, *Phys. Rev. B* **39**, 10552–10559 (1989).
2. D. Ceperley, B. Alder, *Physica B+C* **108**, 875–876 (1981).
3. S. Stishov, *Phys. Uspekhi* **44**, 285–290 (2001).
4. S. A. Bonev, E. Schwegler, T. Ogitsu, G. Galli, *Nature* **431**, 669–672 (2004).

5. E. Babaev, A. Sudbø, N. W. Ashcroft, *Nature* **431**, 666–668 (2004).
6. A. Schuch, E. Grilly, R. Mills, *Phys. Rev.* **110**, 775 (1958).
7. C. L. Guillaume *et al*., *Nat. Phys.* **7**, 211–214 (2011).
8. T. Matsuoka *et al*., *Phys. Rev. B* **89**, 144103 (2014).
9. T. Matsuoka, K. Shimizu, *Nature* **458**, 186–189 (2009).
10. A. M. J. Schaeffer, W. B. Talmadge, S. R. Temple, S. Deemyad, *Phys. Rev. Lett.* **109**, 185702 (2012).
11. A. Lazicki, Y. Fei, R. J. Hemley, *Solid State Commun.* **150**, 625–627 (2010).
12. S. Deemyad, J. S. Schilling, *Phys. Rev. Lett.* **91**, 167001 (2003).
13. V. V. Struzhkin, M. I. Eremets, W. Gan, H. K. Mao, R. J. Hemley, *Science* **298**, 1213–1215 (2002).
14. K. Shimizu, H. Ishikawa, D. Takao, T. Yagi, K. Amaya, *Nature* **419**, 597–599 (2002).
15. A. M. Schaeffer, S. R. Temple, J. K. Bishop, S. Deemyad, *Proc. Natl. Acad. Sci. U.S.A.* **112**, 60–64 (2015).
16. C. S. Barrett, *Phys. Rev.* **72**, 245 (1947).
17. A. W. Overhauser, *Phys. Rev. Lett.* **53**, 64–65 (1984).
18. H. G. Smith, *Phys. Rev. Lett.* **58**, 1228–1231 (1987).
19. A. D. Zdetsis, *Phys. Rev. B* **34**, 7666–7669 (1986).
20. R. J. Gooding, J. A. Krumhansl, *Phys. Rev. B* **38**, 1695–1704 (1988).
21. C. M. McCarthy, C. W. Tompson, S. A. Werner, *Phys. Rev. B* **22**, 574–580 (1980).
22. L. Proville, D. Rodney, M.-C. Marinica, *Nat. Mater.* **11**, 845–849 (2012).
23. A. M. Schaeffer *et al*., *Nat. Commun.* **6**, 8030 (2015).
24. H. G. Smith, R. Berliner, J. D. Jorgensen, M. Nielsen, J. Trivisonno, *Phys. Rev. B* **41**, 1231–1234 (1990).
25. G. Ernst, C. Artner, O. Blaschko, G. Krexner, *Phys. Rev. B* **33**, 6465–6469 (1986).
26. See supplementary materials.
27. D. L. Martin, *Physica* **25**, 1193–1199 (1959).
28. V. S. Kogan, *Sov. Phys. Uspekhi* **5**, 951–975 (1963).
29. W. Schwarz, O. Blaschko, *Phys. Rev. Lett.* **65**, 3144–3147 (1990).
30. J. B. Neaton, N. W. Ashcroft, *Nature* **400**, 141–144 (1999).
31. G. J. Ackland, I. R. Macleod, *New J. Phys.* **6**, 138 (2004).
32. I. Tamblyn, J.-Y. Raty, S. A. Bonev, *Phys. Rev. Lett.* **101**, 075703 (2008).
33. C. J. Pickard, R. J. Needs, *Phys. Rev. Lett.* **102**, 146401 (2009).
34. E. R. Hernández, A. Rodriguez-Prieto, A. Bergara, D. Alfè, *Phys. Rev. Lett.* **104**, 185701 (2010).
35. M. Marqués *et al*., *Phys. Rev. Lett.* **106**, 095502 (2011).
36. P. Souvatzis, O. Eriksson, M. Katsnelson, S. Rudin, *Comput. Mater. Sci.* **44**, 888–894 (2009).
37. W. Schwarz, O. Blaschko, I. Gorgas, *Phys. Rev. B* **44**, 6785–6790 (1991).
38. R. Berliner, S. A. Werner, *Phys. Rev. B* **34**, 3586–3603 (1986).
39. E. L. Gromnitskaya, O. V. Stal'gorova, S. M. Stishov, *JETP Lett.* **69**, 38–43 (1999).
40. R. G. Hennig *et al*., *Nat. Mater.* **4**, 129–133 (2005).
41. R. K. Bollinger *et al*., *Phys. Rev. Lett.* **107**, 075503 (2011).
42. M. Hanfland, K. Syassen, N. E. Christensen, D. L. Novikov, *Nature* **408**, 174–178 (2000).
43. G. J. Ackland, A. Jones, *Phys. Rev. B* **73**, 054104 (2006).
44. U. Pinsook, G. J. Ackland, *Phys. Rev. B* **62**, 5427–5434 (2000).

ACKNOWLEDGMENTS

We thank J. K. Hinton and M. C. MacLean for assistance in data collection; T. Taylor for assistance in data analysis; S. Tkachev and GSECARS for providing the helium gas loading; J. Smith, C. Kenney-Benson, and R. Ferry in 16-ID-B for experimental support; G. Shen and Y. Meng for providing additional beamtime for final measurements; and D. Fernandez, V. Deshpande, and L. Yang for experimental support on sample purity checks. The experimental work was performed at HPCAT (Sector 16), Advanced Photon Source (APS), Argonne National Laboratory. HPCAT operations are supported by DOE-NNSA under award DE-NA0001974 with partial instrumentation funding by NSF. The APS is a U.S. Department of Energy (DOE) Office of Science User Facility operated for the DOE Office of Science by Argonne National Laboratory under contract DE-AC02-06CH11357. Beam time for these experiments was provided by the Carnegie-DOE Alliance Center, which is supported by DOE-NNSA under grant DE-NA-0002006. Research at the University of Utah was supported by NSF Division of Materials Research award 1351986. S.S. acknowledges the support of DOE-BES/DMSE under award DE-FG02-99ER45775. Research at the University of Edinburgh is supported by EPSRC with computing time on EPCC's ARCHER supercomputer (UKCP grant K01465X). G.J.A. was supported by an ERC fellowship "Hecate" and a Royal Society Wolfson fellowship. This work also used resources provided by the Edinburgh Compute and Data Facility [ECDF, www.ecdf.ed.ac.uk; the ECDF is partially supported by the eDIKT initiative (www.edikt.org.uk)]. Experimental data are available in the main text and supplementary materials or are stored in a database on the authors' institution and APS server, which are available from the corresponding author upon reasonable request. Details of computations are available at doi:10.7488/ds/2050.

SUPPLEMENTARY MATERIALS

www.sciencemag.org/content/356/6344/1254/suppl/DC1
Supplementary Text
Materials and Methods
Figs. S1 to S17
Tables S1 to S5
References (*45*–*60*)

29 November 2016; resubmitted 27 January 2017
Accepted 25 May 2017
10.1126/science.aal4886

Science

Quantum and isotope effects in lithium metal

Graeme J. Ackland, Mihindra Dunuwille, Miguel Martinez-Canales, Ingo Loa, Rong Zhang, Stanislav Sinogeikin, Weizhao Cai and Shanti Deemyad

Science **356** (6344), 1254-1259.
DOI: 10.1126/science.aal4886

Lithium gets a new ground state

For the past 70 years, the lowest-energy crystal structure of lithium was believed to be a relatively complex one called the 9R structure. Ackland *et al.* show that this is incorrect. The actual lowest-energy structure for lithium is the much simpler closest-packed face-centered cubic form. In addition, ^{6}Li and ^{7}Li isotopes have crystal phase transitions at slightly different pressures and temperatures. This difference is chalked up to large quantum mechanical effects between the isotopes. Lithium is the only metal that shows this type of quantum effect and presents a challenge for theoreticians to explain.

Science, this issue p. 1254